Quantifying Mechanical Properties in a Murine Fracture Healing System Using an Inverse Geometric Nonlinear Elasticity Modeling Framework

Michael I. Miga[1,2,3], Jared A. Weis[1,4], Froilan Granero-Molto[4], and Anna Spagnoli[4,5]

[1] Vanderbilt University, Department of Biomedical Engineering, Nashville, TN, USA
{Michael.I.Miga, Jared.A.Weis}@vanderbilt.edu
[2] Vanderbilt University Medical Center, Department of Radiology and Radiological Sciences
[3] Vanderbilt University Institute for Imaging Science, Nashville, TN, USA
[4] University of North Carolina at Chapel Hill, Department of Pediatrics
granerof@email.unc.edu
[5] Department of Biomedical Engineering, Chapel Hill, NC, USA
anna_spagnoli@med.unc.edu

Abstract. Understanding bone remodeling and mechanical property characteristics is important for assessing treatments to accelerate healing or in developing diagnostics to evaluate successful return to function. The murine system whereby mid-diaphaseal tibia fractures are imparted on the subject and fracture healing is assessed at different time points and under different therapeutic conditions is a particularly useful model to study. In this work, a novel inverse geometric nonlinear elasticity modeling framework is proposed that can reconstruct multiple mechanical properties from uniaxial testing data. This is investigated within the context of a murine cohort (n=3) that are 14 days post fracture. This work is the first to report mechanical properties of a callus using an inverse problem methodology whereby 2758.4 ± 682.5 kPa, 0.467 ± 0.009 were found to be the Young's modulus and Poisson's ratio, respectively. In addition better consistency of the reconstructed metrics over more traditional metrics is demonstrated.

Keywords: fracture healing, murine, finite element, inverse problems, elasticity.

1 Introduction

There is significant morbidity and mortality due to the improper or inhibited healing of bone fractures and is especially relevant to the aging population [1-3]. Restoration of mechanical function to bone is an important healthcare concern and processes to accelerate that process or mediate more successful outcomes is of high significance. In addition, the development of diagnostics that can assess the mechanical function of bone are equally important. Murine systems have become natural platforms for the investigation of therapeutics towards improved healing [4] and ex vivo mechanical testing has served as the primary means to assess efficacy [5, 6]. However, due to confounding geometric effects associated with callus growth and remodeling, robust metrics of evaluation are challenging.

F. Bello and S. Cotin (Eds.): ISBMS 2010, LNCS 5958, pp. 29–37, 2010.

To address this, investigators have begun to explore using the detailed structure provided by microCT imaging to facilitate general imaging metrics as well as computational approaches to assess mechanical function using more subject specific models/metrics [7-11]. In this paper, an approach is investigated which looks at the problem more within the context of an inverse problem approach. Similar to work by Shefelbine et al. [9] and Weis et al. [10, 11], a finite element framework is used to generate subject-specific callus models. In this work, an inverse methodology is investigated which represents a significant advance to addressing the problem with computational techniques.

2 Methods

2.1 Inverse Geometric Nonlinear Elasticity Modeling Framework

Hooke's Law is a widely used constitutive law to represent the stress-strain behavior of a material. In the case of uniaxial loading (Figure 1), the full strain state can be expressed with respect to the applied force as shown here,

$$\varepsilon_x = \frac{\sigma_x}{E}, \varepsilon_y = -\nu\frac{\sigma_x}{E}, \varepsilon_z = -\nu\frac{\sigma_x}{E}, \gamma_{xy} = \gamma_{xz} = \gamma_{yz} = 0 \quad (1)$$

where E is Young's modulus and often referred to as the stiffness, and ν is Poisson's ratio which represents the negative ratio of transverse to axial strain. When conducting mechanical testing, the traditional technique is to prepare a sample with known shape such that the cross-sectional area, A, and reference length, L, are known, and the displacements and forces applied are measured by the testing device. This allows one to take that data and calculate the stiffness of the specimen with, $E = \frac{FL}{A\delta}$ where F is the measured force for the given displacement δ. Typically with this approach a series of displacements are used that span the small strain region of the material characteristic curves and a modulus is fit.

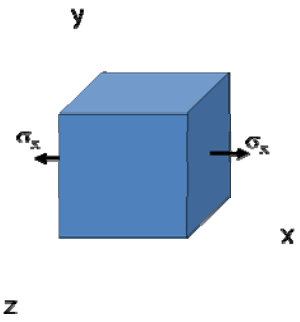

Fig. 1. Uniaxial loading

Of course, the reality is that with the application of an increment of displacement, a change to the cross-sectional area (via Poisson's ratio) is imparted and ultimately affects the measured force. This nonlinear effect is due to the specimen changing shape. To demonstrate, in a simple analytical experiment, a 1 cm cube under tensile loading experienced strains from 0-10% with E=1 MPa (a reasonable approximation to callus stiffness) and a Poisson's ratio of ν=0.3. Figure 2a illustrates the two respective stress-strain curve where 'L' and 'GNL' represent the linear and geometrically nonlinear approaches, respectively. Figure 2b demonstrates the difference in force when taking geometric nonlinearity into account over a range of Poisson's ratio. This is produced by incrementally deforming the specimen cube and accumulating the force at each increment, which is a common strategy to linearize geometric nonlinear

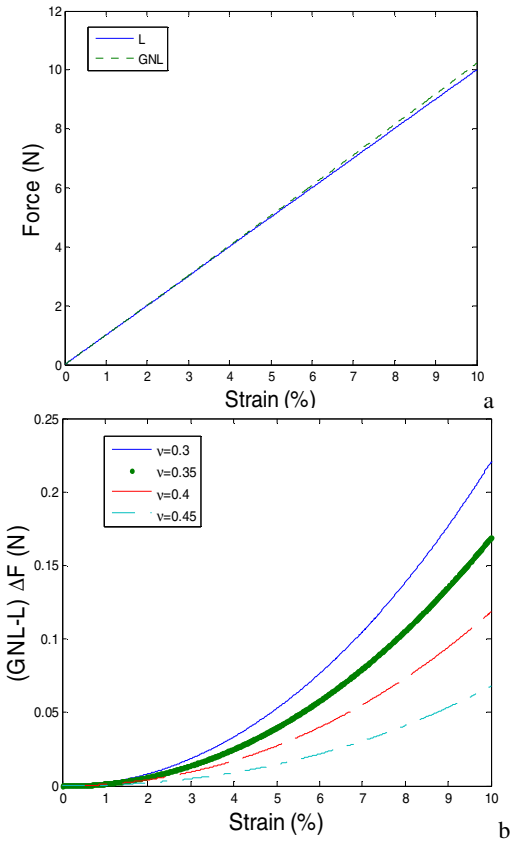

Fig. 2. (a) Force vs strain for linear and geometrically nonlinear problems, (b) the difference in force values over several Poisson's ratios.

changes are expected than the homogeneous example discussed above. In addition, for this paper the callus is being 'lumped', i.e. characterized, as one region with unique mechanical properties. Figure 3 illustrates the typical callus region extracted from μCT data and its geometrical complexity consisting of cartilage (red), new bone (blue), and highly mineralized bone (white). As a dynamic grid finite element model is implemented under tensile load, one can easily note that the geometric relationships between these callus constituents will rapidly change which will manifest in changes to the incremental force.

For the purpose of reconstructing multiple material parameters for the callus region, the problems. As can be seen in Figure 2b, a distinctive force versus strain curve is generated for each Poisson's ratio. This is directly related to the geometric changes to cross-sectional area as reflected by varying Poisson's ratios.

We hypothesize that by taking into account geometrically nonlinear effects within an inverse reconstruction framework that multiple properties can be differentiated from uniaxial testing data. More specifically, we propose to model the geometric nonlinearity in a similar manner as the above analytic example whereby with each increment we deform the mesh and then impart the next increment. The measured forces are then determined by summing the increments. For the application herein concerned with the mechanical integrity of a healing callus, more dramatic

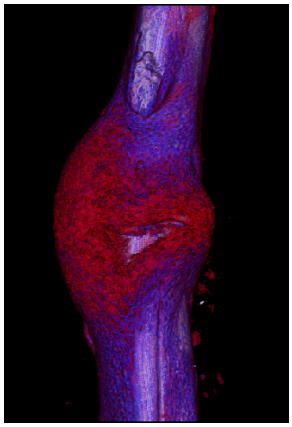

Fig. 3. Image showing callus consistency. Rendering utilizes transparency to reflect bone composition with (red) cartilage, (blue) new bone, and (white) highly mineralized bone.

model for mechanical equilibrium will be expressed in terms of Lame' constants and is stated here,

$$G\nabla^2\bar{u} + (G+\lambda)\nabla(\nabla \bullet \bar{u}) = 0, \tag{2}$$

where G is the shear modulus, λ is the second Lame' constant, and $\bar{u}$ is the displacement vector. With an initial guess at these material parameters, a finite element model of the domain shown in Figure (3) can be constructed, analogous displacements are imposed that match the experimental conditions, and an average force (F_{calc}) is reconstructed from the simulation. A custom-built Levenberg-Marquardt non-linear optimization algorithm is then used to iteratively optimize the material properties such that F_{calc} approaches the experimental material tester generated force (F_{exptl}). In this approach, each strain level is treated as an independent data point with respect to determining the mechanical properties. The important aspect to the approach is that each strain state represents an accumulation effect associated with approximating the geometric nonlinearity. Ultimately this translates to the objective function,

$$\Psi(G,\lambda) = \sum_{i=1}^{N} \left(F_{calc} - F_{exptl}\right)_i^2 \tag{3}$$

where N is the number of displacement data points along the elastic region of the force-displacement curve. The goal is to minimize this objective function with respect to two mechanical properties, G and λ, of the 'lumped' callus region. To optimize this for the callus properties, the derivative of our objective function, $\Psi(G,\lambda)$, is taken with respect to the properties G and λ, and set equal to zero, i.e.

$$\begin{bmatrix} \frac{d\Psi(G,\lambda)}{dG} \\ \frac{d\Psi(G,\lambda)}{d\lambda} \end{bmatrix} = \begin{bmatrix} \frac{\partial F_{calc1}}{\partial G} & \frac{\partial F_{calc2}}{\partial G} & \cdots & \frac{\partial F_{calcN}}{\partial G} \\ \frac{\partial F_{calc1}}{\partial \lambda} & \frac{\partial F_{calc2}}{\partial \lambda} & \cdots & \frac{\partial F_{calcN}}{\partial \lambda} \end{bmatrix} \begin{Bmatrix} F_{calc1} - F_{exptl1} \\ F_{calc2} - F_{exptl2} \\ \vdots \\ F_{calcN} - F_{exptlN} \end{Bmatrix} = \begin{bmatrix} 0 \\ 0 \end{bmatrix}, \tag{4}$$

or simplified as,

$$[J]^T \{\bar{F}_{calc} - \bar{F}_{exptl}\} = 0 \tag{5}$$

where [J] is the Jacobian matrix. It is important to note that in the above equation each component of the Jacobian is independent and is built over a series of incremental developments. In the case of a fixed mesh/grid counterpart to this approach, each subsequent strain state is just a scalar multiple based on the applied deformations (i.e. double the applied deformation, and double the Jacobian term). The relationship between force and property is just a linear function of applied displacement. However in the GNL approach, each increment provides new information regarding the geometric relationship of the callus constituents. The result is that the standard Levenberg-Marquardt framework contains considerably more information and can be implemented such that multiple mechanical property reconstruction is possible, i.e.

$$\left([J]^T[J] + \alpha I\right)[\Delta\bar{P}] = [J]^T\{\bar{F}_{calc} - \bar{F}_{exptl}\}, \tag{6}$$

and

$$[\Delta\bar{P}] = \begin{bmatrix} G \\ \lambda \end{bmatrix}_{i+1} - \begin{bmatrix} G \\ \lambda \end{bmatrix}_i, \tag{7}$$

with the regularization term α defined as,

$$\alpha = \left(\phi * \text{trace}\left([J]^T [J]\right) * SSE^2\right)^{1/2} \quad (8)$$

[12], where ϕ is an empirical factor, and SSE is the sum squared error between measured and calculated force. It should be noted that the Jacobian was determined by a finite difference calculation which was initiated by a 2.5% perturbation from the initial guess of the callus property. The process is iterative until the relative error between iterations converges below a set tolerance or until no improvement in objective function is noted. With respect to reporting the values in this paper, the Lame' constants were converted to Young's modulus and Poisson's ratio for the purpose of comparing with the more traditional metrics. In addition, two other reconstructions were executed whereby Poisson's ratio was fixed (ν=0.45) and Young's modulus was determined using the linear and geometric nonlinear approaches for a single property.

2.2 Murine System

Three female syngenic FVB mice (FVB-NJ, Jackson Laboratories) 8 to 12 weeks old with a pin-stabilized mid-diaphaseal tibia fracture were generated. Procedural implementation utilized a standard three point bending system for fracture delivery [13], anesthesia, and pain control and was approved by the Institutional Animal Care and Use Committee at Vanderbilt University Medical Center and the University of North Carolina at Chapel Hill. At day 14, the mice were euthanized and tibia fractures were dissected, and wrapped in phosphate buffered saline (PBS) soaked gauzed. The specimens were then placed within a Scanco μCT 40 scanner (Scanco Medical) and an approximate 5 mm section was scanned for each specimen which consisted of callus and bone ends. Once completed, each specimen was prepared for mechanical testing by embedding each end within a customized polymethylmethacrylate cast such that it could be placed within the testing unit while also allowing the callus to remain exposed and free of constraints. The assembly was placed with an Enduratec Electroforce 3100 mechanical tester (Bose, Enduratec Systems Group) and tested in tension at a fixed displacement rate of 0.25 mm/min using a 22 N force transducer (Honeywell Sensotec). Data consisted of displacement and force values and was recorded continuously until failure. Figure 4 shows a murine tibia being tested.

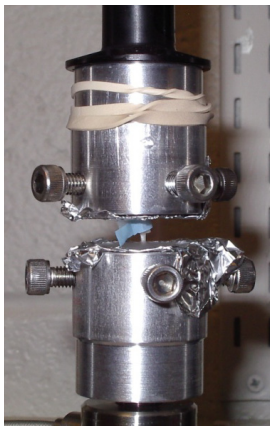

Fig. 4. A murine mouse tibia loaded within the testing apparatus

Once the collection of the imaging and displacement data is complete, the bone/callus regions are segmented from the μCT data, a tetrahedral grid is generated, and properties are assigned to mineralized bone and void regions. In this work, highly mineralized bone (white regions in Figure 3) were assigned E=5 MPa, and ν=0.3 MPa [14], while voids within the domain were assigned negligible material properties. With the computational model and data in place, these are then provided to the inverse approach. In this paper, three inverse approaches are generated: (1) a single callus shear modulus reconstruction using the static mesh, (2) a single callus

shear modulus value using the dynamic grid, and (3) a dual callus reconstruction of the Lame' constants using the dynamic grid. In addition, the apparent stiffness, and normalized apparent stiffness are reported which are common metrics within the literature. Apparent stiffness is the slope of the best fit line to force versus displacement data within the linear loading phase. Normalized apparent stiffness is the same fitting procedure but with the force and displacement values normalized by the largest cross-sectional area of the callus and overall length, respectively.

3 Results

Figure 5 illustrates a typical result from the model generation process. Figure 6 illustrates the force versus displacement curves for all (n=3) mice. Table 1 reports the

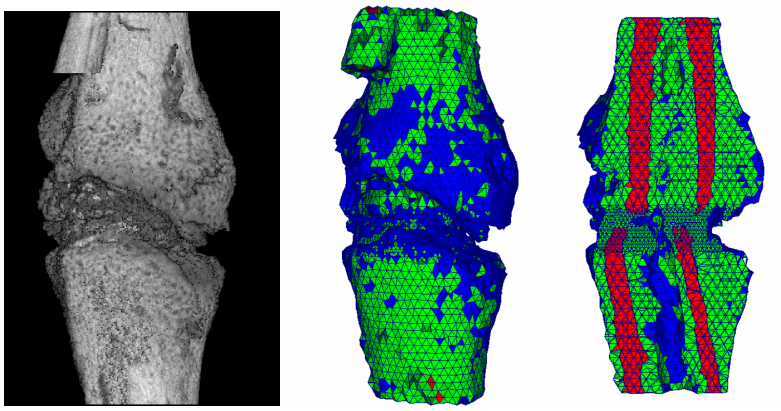

Fig. 5. (left) Volume rendered μCT of callus, (middle) tetrahedral grid of volume, (right)

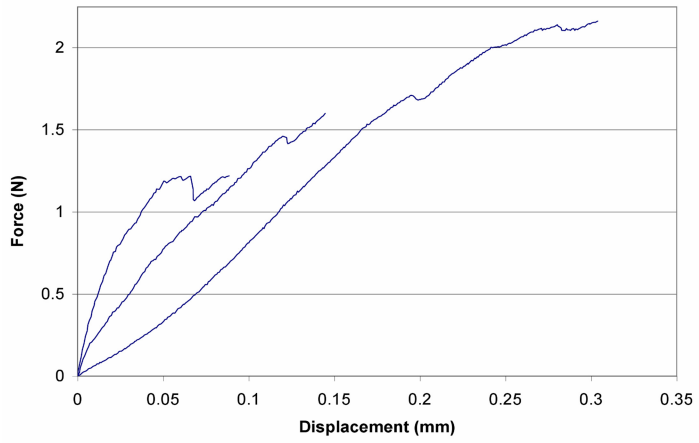

Fig. 6. Force versus displacement for (n=3) mice. Only regions prior to an approximate elastic limit were analyzed as part of the reconstructive analysis.

Table 1. Metrics for mechanical properties assessed over (n=3) mice

PROPERTY	14 d (n=3)	SD as % of mean
Apparent Stiffness (N/mm)	13.95 ± 6.24	44.7%
Normalized Apparent Stiffness (kPa)	8330.1 ± 4941.0	59.3%
$E_{reconstructed}$ (kPa) Linear (ν=0.45 fixed)	2908.3 ± 872.8	30.0%
$E_{reconstructed}$ (kPa) Geometric NonLinear (ν=0.45 fixed)	3230.2 ± 986.7	30.5%
$E_{reconstructed}$ (kPa), $\nu_{reconstructed}$ Geometric NonLinear (dual property)	2758.4 ± 682.5, 0.467 ± 0.009	24.7%, 1.9%

mechanical property metric types in the first column with their corresponding value in the second column. While statistical significance from such a small data set cannot be achieved at this time it is interesting to look at the magnitude of the standard deviations relative to the mean property across the different metrics (reported in column 3 of Table 1).

4 Discussion

The methods reported have shortcomings at this early stage but nevertheless the results are promising. Some of those short comings are: (1) lack of finer discretization of the callus models as shown in Figure 5, (2) the choice of tetrahedral elements as opposed to ones more accurate in mechanics modeling, e.g. hexahedral elements [15], (3) although the grid is dynamic in the geometric nonlinear approach, the lack of re-meshing for the intermediate steps to ensure optimal element aspect ratios, (4) the high strain conditions within the fracture fissure likely need the full-nonlinear strain tensor description, (5) lack of more data necessary to achieve statistical significance, and (6) the inherent experimental error associated with 'potting' tibia fractures and mechanical testing. Despite this however, it is encouraging that the reconstructed values are quite consistent among the widely distributed force/displacement curves. The heterogeneity among these curves can be seen in the considerably large standard deviation of the apparent stiffness and the normalized apparent stiffness as compared to their mean values. Comparing quantitatively, the standard deviations of the apparent stiffness values are approximately 45-60% relative to the mean value while reconstructed values using the inverse approaches are only 25-30% of the mean. This suggests that model-based inverse analysis produces a more consistent metric. The considerable 15% increase in variation when normalizing the apparent stiffness suggests that the process of normalization introduces variability and would seem to confirm the confounding effects of geometry often referred to in the literature. The contribution of the work is that this represents to our knowledge the only inverse elasticity approach to this problem. Because the approach is based on measured force, each result from the three variants to

the algorithm represents a quantitative value. As the shortcomings are overcome, better absolute quantification will be achieved, but even as realized here, the approach may serve as an effective means to differentiate and score different treatment groups at different time points. In fact, in recent work not reported here, the ability to differentiate different time (10 day, 14 day post-fracture) points of healing under similar fracture conditions has been found in an expanded cohort (n=6) of mice. Interestingly, the reconstructive analysis was the only method to find statistical significance among the two groups [11].

5 Conclusion

This paper presents a novel inverse approach that takes advantage of geometric nonlinearities to increase the extent of information such that the reconstruction of multiple material properties is achieved. It also goes on to compare different realizations of the approach and compares these to more common metrics to qualify mechanical properties in a murine fracture system. The results indicate a more consistent result across mice using the model-based analysis. Future work will involve investigating if the method can be used to differentiate mice at different healing points and among different treatments.

Acknowledgments. This work was supported by National Institutes of Health (NIH) Grant 5R01DK070929-02 from the National Institute of Diabetes and Digestive and Kidney Diseases (NIDDK).

References

1. Tomak, Y., Kocaoglu, M., Piskin, A., Yildiz, C., Gulman, B., Tomak, L.: Treatment of intertrochanteric fractures in geriatric patients with a modified external fixator. Injury-International Journal of the Care of the Injured 36, 635–643 (2005)
2. Toh, E.M., Sahni, V., Acharya, A., Denton, J.S.: Management of intracapsular femoral neck fractures in the elderly; is it time to rethink our strategy? Injury-International Journal of the Care of the Injured 35, 125–129 (2004)
3. Sharif, K.M., Parker, M.J.: Austin Moore hemiarthroplasty: technical aspects and their effects on outcome, in patients with fractures of the neck of femur. Injury-International Journal of the Care of the Injured 33 (2002); PII S0020-1383(0002)00041-00044
4. Granero-Molto, F., Weis, J.A., Landis, B., Longobardi, L., Miga, M.I., Spagnoli, A.: Mesenchymal Stem Cells Enhance Fracture Healing: Essential Role for Cytokines in Homing and Anti-Inflammatory Response. Journal of Bone and Mineral Research 23, S166–S167 (2008)
5. Gardner, M.J., van der Meulen, M.C.H., Demetrakopoulos, D., Wright, T.M., Myers, E.R., Bostrom, M.P.: In vivo cyclic axial compression affects bone healing in the mouse tibia. J. Orthop. Res. 24, 1679–1686 (2006)
6. Moukoko, D., Pithioux, M., Chabrand, P.: Temporal evolution of mechanical properties of skeletal tissue regeneration in rabbits: an experimental study. Med. Biol. Eng. Comput. 45, 989–995 (2007)

7. Morgan, E.F., Mason, Z.D., Chien, K.B., Pfeiffer, A.J., Barnes, G.L., Einhorn, T.A., Gerstenfeld, L.C.: Micro-computed tomography assessment of fracture healing: Relationships among callus structure, composition, and mechanical function. Bone 44, 335–344 (2009)
8. Reynolds, D.G., Hock, C., Shaikh, S., Jacobson, J., Zhang, X.P., Rubery, P.T., Beck, C.A., O'Keefe, R.J., Lerner, A.L., Schwarz, E.M., Awad, H.A.: Micro-computed tomography prediction of biomechanical strength in murine structural bone grafts. J. Biomech. 40, 3178–3186 (2007)
9. Shefelbine, S.J., Simon, U., Claes, L., Gold, A., Gabet, Y., Bab, I., Muller, R., Augat, P.: Prediction of fracture callus mechanical properties using micro-CT images and voxel-based finite element analysis. Bone 36, 480–488 (2005)
10. Weis, J.A., Granero-Molto, F., O'Rear, L.D., Miga, M.I., Spagnoli, A.: Development of a high-resolution 3D Micro-CT based model to predict fracture callus histological architecture. Journal of Bone and Mineral Research 22, W472 (2007)
11. Weis, J.A., Miga, M.I., Granero-Molto, F., Spagnoli, A.: A finite element inverse analysis to assess functional improvement during the fracture healing process. J. Biomech. (in press, 2009)
12. Joachimowicz, N., Pichot, C., Hugonin, J.P.: Inverse Scattering - an Iterative Numerical-Method for Electromagnetic Imaging. IEEE Transactions on Antennas and Propagation 39, 1742–1752 (1991)
13. Bonnarens, F., Einhorn, T.A.: Production of a standard closed fracture in laboratory animal bone. J. Orthop. Res. 2, 97–101 (1984)
14. Schriefer, J.L., Robling, A.G., Warden, S.J., Fournier, A.J., Mason, J.J., Turner, C.H.: A comparison of mechanical properties derived from multiple skeletal sites in mice. J. Biomech. 38, 467–475 (2005)
15. Benzley, S.E., Perry, E., Merkley, K., Clark, B., Sjaardema, G.: A Comparison of All-Hexahedral and All-Tetrahedral Finite Element Meshes for Elastic and Elasto-Plastic Analysis. In: Proc. 4th International Meshing Roundtable, Sandia National Laboratories, pp. 179–191 (1995)